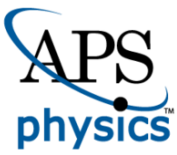

Relativistic tidal effects in nonstandard Kerr spacetime

Andrea Maselli, Kostas Kokkotas, and Pablo Laguna

Phys. Rev. D **93**, 064075 — Published 29 March 2016

DOI: 10.1103/PhysRevD.93.064075

Relativistic tidal effects in non standard Kerr space-time

Andrea Maselli,[1,*] Kostas Kokkotas,[1,2,†] and Pablo Laguna[2,‡]

[1] *Theoretical Astrophysics, Eberhard Karls University of Tuebingen, Tuebingen 72076, Germany*
[2] *Center for Relativistic Astrophysics and School of Physics, Georgia Institute of Technology, Atlanta, Georgia 30332, USA*

Astrophysical phenomena involving massive black holes (BHs) in close binaries are expected to leave detectable signatures in the electromagnetic and gravitational-wave spectrum. Such imprints may provide precious information to probe the space-time around rotating BHs, and to reveal new insights on the nature of gravity in the strong-field regime. To support this observational window it is crucial to develop suitable tests to verify the predictions of General Relativity (GR). In this framework, the metric recently proposed by Johannsen and Psaltis parametrises strong field deviations from a Kerr space-time in a theory-independent way. In the following, we make use of this approach to describe the tidal field produced by spinning BHs. We compute the gravito-magnetic and gravito-electric tidal tensors for particles moving on equatorial circular geodesics, comparing our results with those obtained in the standard GR scenario. Our calculations show significant differences even for distances far form the last stable orbit, which may affect the evolution of the binary and leave detectable signatures. We test our framework computing quasi-equilibrium sequences of BH-WD systems by means of the affine model, for different binary configurations.

PACS numbers: 04.50.Kd, 04.70.-s

I. INTRODUCTION

Since its formulation one hundred years ago, General Relativity has successfully passed a large set of observational and experimental tests [1]. Most of them however, probed only the weak field regime of gravity, and therefore a number of strong-field GR predictions still remain to be verified [2–5]. Black holes are among the most genuine of such predictions, with no analog in the Newtonian theory, and represent the ideal candidates to test gravity under extreme conditions. In General Relativity BHs belong to the Kerr family, and according to the no-hair theorem, their exterior stationary and isolated gravitational field depends only on two parameters: their mass and angular momentum [6]. Initial deviations from the Kerr metric are rapidly radiated away by the emission of gravitational radiation [7]. A proof of the validity of the no-hair theorem is still lacking. However, future electromagnetic [8–11] and gravitational-wave [12, 13] observations promise to shed new light on this scenario, and are expected to prove the *Kerr hypothesis*. In this regard, several efforts have been devoted to develop independent tests to determine the features of the strong gravitational field in the BH surroundings. Such tests follow a bottom-up approach, in which the BH space-time is parametrised in a phenomenological way, with the aim to map possible detected deviations in terms of an alternative theory of gravity. Requiring that the new metric is free of pathologies as naked singularities or closed time-like curves, make these studies an extremely difficult task. We refer the reader to [14] and references therein, for a systematic study of the main features of some parametric frameworks which have been proposed in literature.

In this work, we make use of the new approach recently developed by Johannsen and Psaltis (JP) [15]. The authors introduced polynomial corrections into the Schwarzschild metric as initial seeds, showing that this ansatz can be turned into a Kerr-like metric through the Newmam-Janis algorithm [16]. The mathematical properties and the topology of JP metric, as well as their astrophysical implications have been extensively studied in [14, 15, 17–19]. Moreover, tests involving properties of iron lines, quasi periodic oscillations, continuum spectra of accretion disks and images of the accretion flows have been analysed in [20–25]. This metric has been also extended to a more general parametrisation in [26], where the authors addressed some un-explored key features of the original framework.

In this paper we investigate the effects of strong-gravity corrections captured by the JP approach, on the tidal field produced by rotating BHs. We derive the expressions for the gravito-magnetic and gravito-electric tidal tensors, which act as source of the geodesic deviation of nearby test particles, and determine the frame-dragging precession of test-gyroscopes. The results of this work can be useful to devise tests of GR through astrophysical observations of close binaries involving a massive BHs and a companion star. Such environments may lead to tidal disruption events even at large distances, producing detectable gravitational and X-ray/UV radiation [27].

In order to test our theoretical framework, we simulate the orbital evolution of BH-WD binaries, using the new formulation of the gravito-electric tidal tensor together with the affine model, which is a semi-analytical approach to describe star deformations induced by an external quadrupolar tidal field. Originally developed to study the evolution of normal stars or WDs within a

* andrea.maselli@uni-tuebingen.de
† kostas.kokkotas@uni-tuebingen.de
‡ plaguna@gatech.edu

Newtonian scheme [28–30], this model was recently improved to describe neutron star tidal disruption events in compact binaries, taking into account relativistic effects on the stellar structure [31, 32], and post-Newtonian corrections both on the orbital dynamics and the tidal field [33, 34].

With this framework, we follow quasi-equilibrium sequences of prototype BH-WD binaries for different modified Kerr metrics, finding that the stellar deformations may vary with respect to the GR case up to 5% even for large distances. For each binary configuration we also identify the onset of the mass transfer from the star to the companion object, which can be used as initial data for fully relativistic numerical simulations, to investigate the properties of the accreting flow onto the BH.

This paper is organised as follows. In Section II we introduce the JP metric and we derive the basic features of geodesic motion. In Section III we describe the procedure to characterise the tidal field in the JP space-time, and we explicitly compute the gravito-magnetic and gravito-electric tidal tensors. Moreover, we discuss the relevance of the corrections induced by the strong-gravity modifications of the Kerr metric, comparing our analytical results with those obtained for the pure GR scenario. In Section IV we numerically investigate tidal disruption events in BH-WD binaries, for different configurations. Finally, in Section V we draw the conclusions.

We use Greek letters $(\alpha, \beta, \ldots)$ to denote space-time indices, and Latin characters $(i, j, \ldots)$ for spatial indices.

II. THE JP METRIC

The Johannsen-Psaltis metric is described in Boyer-Lindquist coordinates $x^\mu = (t, r, \theta, \phi)$ by the following line element

$$\begin{aligned} ds^2 =& -(1+h)\left(1-\frac{2Mr}{\Sigma}\right)dt^2 + \frac{\Sigma(1+h)}{\Delta + a^2\sin^2\theta h}dr^2 \\ &+ \Sigma d\theta^2 - \frac{4aMr\sin^2\theta}{\Sigma}(1+h)dtd\phi \\ &+ \left[r^2 + a^2 + \frac{2a^2Mr\sin^2\theta}{\Sigma} + h\frac{a^2(\Sigma+2Mr)}{\Sigma}\sin^2\theta\right] \\ &\times \sin^2\theta d\phi^2 \ , \end{aligned} \tag{1}$$

where $\Sigma = r^2 + a^2\cos^2\theta$ and $\Delta = r^2 + a^2 - 2Mr$. The function $h(r, \theta)$ parametrizes the deviations from the *pure* Kerr space-time, and is given by

$$h(r,\theta) = \sum_{k=0}^{\infty}\left(\epsilon_{2k} + \epsilon_{2k+1}\frac{Mr}{\Sigma}\right)\left(\frac{M^2}{\Sigma}\right)^k \ . \tag{2}$$

The JP metric has an infinite number of deformations parameters. However, some of them are constrained by theoretical and experimental bounds. As noted in [26], the requirement $\epsilon_0 = 0$ represents a sufficient condition to guarantee that Eq. (1) satisfies asymptotic flatness at spatial infinity. Moreover, limits on the coefficients $\epsilon_{1,2}$ can be obtained from weak-field tests of gravity within the parametrized post-Newtonian framework, performed in the Solar System [35]. Such bounds translate into $|\epsilon_1| \lesssim 10^{-5}$ and $|\epsilon_2| \lesssim 4.6 \times 10^{-4}$ [15].

In this work we assume ϵ_3 as the only non vanishing parameter of $h(r, \theta)$. Such coefficient is currently unconstrained by observations and reflect changes of the Kerr metric at the order $\sim (M/r)^3$. We also focus on the orbital motion of massive test-particles on equatorial circular geodesics, for which $\theta = \pi/2$. This condition further reduces Eq. (2) to

$$h = \epsilon_3\frac{M^3 r}{\Sigma^2} = \epsilon_3\frac{M^3}{r^3} \ . \tag{3}$$

Finally, we consider the strong-field effects identified by h, as small perturbations of the Kerr geometry, i.e. $\epsilon_3 M^3/r^3 \ll 1$. We develop our framework at the linear approximation, neglecting $\mathcal{O}(h^2)$ corrections. The typical values ϵ_3 considered in literature so far to analyse possible signatures of the JP metric are of the order $\sim \mathcal{O}(10)$ [14, 15, 20–22, 26]. As shown in Fig. 1, for such values, the condition $h \ll 1$ is satisfied whenever the test-particle orbits around the black hole at distances greater than $r \sim 6M$. This requirement is consistent with the study of astrophysical systems composed of a supermassive black hole and a solar-type star or a white dwarf, which are the primary target of our analysis [36]. It is worth remarking that the parameter ϵ_3 is expected

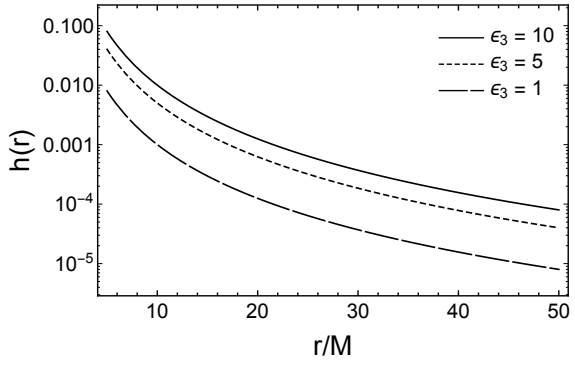

Figure 1. We show the behaviour of $h(r)$ of Eq. (3) as function of the orbital distance normalised to the BH mass, for three values of the parameter $\epsilon_3 = (1, 5, 10)$.

to modify the BH quadrupole moment. This could affect the properties of geodesics around the central objects, varying the nodal precession frequency [37–39], or leading to vertical instabilities in the orbits [40, 41].

The JP metric Eq. (1) is characterised by two killing vectors k^μ and m^μ associated to the space-time invariance with respect to time-shifts and rotations along the polar angle ϕ. The orbital motion of a test-particle with 4-velocity $u^\mu = dx^\mu/d\tau = (u^t, 0, 0, u^\phi)$, being τ the proper time, is then featured by two conserved quant-

ities related to k^μ and m^μ:

$$u^\mu k_\mu = u^t g_{tt} + u^\phi g_{t\phi} = -\mathcal{E} \ , \tag{4}$$

$$u^\mu m_\mu = u^\phi g_{\phi\phi} + u^t g_{t\phi} = L \ . \tag{5}$$

which can be identified with the energy at infinity and the angular momentum for mass unit of the test-particle, respectively. An analytic expressions for $\mathcal{E}$ and L may be derived solving the system of equations $V_{\rm eff} = 0$ and $V'_{\rm eff} = 0$,where

$$V_{\rm eff}(r) = \frac{1}{g_{rr}}\left[\frac{g_{\phi\phi}\mathcal{E}^2 + 2g_{t\phi}\mathcal{E}L + g_{tt}L^2}{g_{t\phi}^2 - g_{tt}g_{\phi\phi}} - 1\right] \ , \tag{6}$$

is an effective potential governing the geodesic motion of a stationary and axisymmetric space-time [42]. From Eqns. (6) and its derivative, we obtain at the linear order in h:

$$\mathcal{E} = \frac{1}{N}\left(1 - \frac{2M}{r} + a\omega_{\rm k}\right) - \frac{h}{N^3}\left[\frac{3}{4}\frac{a^2}{r^2} + \frac{1}{4} - ar^2\omega_{\rm k}^3 - \frac{\omega_{\rm k}^2}{2}(r^2+6a^2) + \frac{3}{2}\frac{a^3}{r^2}\omega_{\rm k}\right] \ , \tag{7}$$

and

$$L = \frac{r^2\omega_{\rm k}}{N}\left(1 + \frac{a^2}{r^2} - 2a\omega_{\rm k}\right) - \frac{h}{N^3}\left[r^2(a^2+3r^2)\omega_{\rm K}^3 + \left(\frac{3a^4}{2r^2} - a^2 - 3r^2\right)\omega_{\rm k} + \frac{3}{4\omega_{\rm k}}\left(1 + \frac{a^2}{r^2}\right) - \left(3a^3 + \frac{9ar^2}{2}\right)\omega_{\rm K}^2 + \frac{9a}{4r^2}(r^2+a^2)\right] \ , \tag{8}$$

where $\omega_{\rm k} = (M/r^3)^{1/2}$ is the *Keplerian* orbital frequency, and we have defined $N = (1+2a\omega_{\rm k} - 3r^2\omega_{\rm k}^2)^{1/2}$. Replacing the former expressions into Eqns. (4)-(5) leads to the 4-velocity components u^t and u^ϕ:

$$u^t = \frac{1+a\omega_{\rm k}}{N} - \frac{h}{N^3 4r^2}\left[3a^2 + 5r^2 + 6a(a^2+r^2)\omega_{\rm k} - 4r^2(4a^2+3r^2)\omega_{\rm K}^2 + 12ar^4\omega_{\rm k}^3\right] \ , \tag{9}$$

$$u^\phi = \frac{\omega_{\rm k}}{N} - \frac{h}{4r^2\omega_{\rm k}N^3}\left[6a^2\omega_{\rm k}^2 + a\omega_{\rm k}(9 - 16r^2\omega_{\rm k}^2) + 3(1-2r^2\omega_{\rm k}^2)^2\right] \ . \tag{10}$$

III. THE TIDAL FIELD

In GR the effects of the stationary gravitational field is described by tidal forces acting on test masses. Single geodesics can not detect gravity and at least a pair of them is needed. In presence of a mass M the space-time is equipped with a metric $g_{\mu\nu}$ and a test-body with 4-velocity u^μ will follow time-like geodesics of this metric. If we assume a second test particle, which position with respect to the first one is defined by the displacement vector δx^μ, we can study the relative motion between them using a quasi-inertial Fermi coordinate system [43]. For this purpose, let's consider an orthonormal tetrad[1] $\lambda^\mu{}_{(\alpha)}$ attached to m (which stays forever at the origin of this coordinate frame), parallel transported along its geodesic parametrised by the proper time τ. In Fermi coordinates, the metric at the second order in the displacement vector $y^{(i)} = \lambda^{(i)}{}_\mu \delta x^\mu$ will be given by:

$$g_{00} = -1 - R_{(0)(i)(0)(j)}y^{(i)}y^{(j)} + \dots \ , \tag{11}$$

$$g_{0i} = -\frac{2}{3}R_{(0)(j)(i)(k)}y^{(j)}y^{(k)} + \dots \ , \tag{12}$$

$$g_{ij} = \delta_{ij} - \frac{1}{3}R_{(i)(k)(j)(l)}y^{(k)}y^{(l)} + \dots \ , \tag{13}$$

where $R_{(\mu)(\nu)(\rho)(\sigma)}$ is the projection of the Riemann curvature tensor onto the orthonormal tetrad frame

$$R_{(\mu)(\nu)(\rho)(\sigma)} = R_{\alpha\beta\gamma\delta}\lambda^\alpha{}_{(\mu)}\lambda^\beta{}_{(\nu)}\lambda^\gamma{}_{(\rho)}\lambda^\delta{}_{(\sigma)} \ . \tag{14}$$

From this equation we can define the *gravito-electric* and *gravito-magnetic* tidal tensors:

$$\mathcal{E}_{(i)(j)} = R_{(0)(i)(0)(j)} \ , \tag{15}$$

$$\mathcal{H}_{(i)(j)} = -\frac{1}{2}\epsilon_{ikl}R^{(k)(l)}{}_{(0)(j)} \ , \tag{16}$$

being ϵ_{ijk} the Levi-Civita symbol. The electric component $\mathcal{E}_{(i)(j)}$ describes tidal deviations of nearby geodesics, while the magnetic term $\mathcal{H}_{(i)(j)}$ is directly related to frame dragging effects of test-gyroscopes. Both tensors are symmetric and trace-free. This set up is physically equivalent, in case of negligible Fermi velocity, to solve the geodesic deviation equation, which can be written in the tetrad frame $\lambda^\mu{}_{(\alpha)}$ as [44]:

$$\frac{d^2 y_{(i)}}{d\tau^2} + \mathcal{E}_{(i)(j)}y^{(j)} = 0 \ . \tag{17}$$

In this section, we shall derive the expressions for Eqns. (15)-(16) in the JP metric, following the approach adopted [43]. To determine the parallel transported vectors $\lambda^\mu{}_{(\alpha)}$ we first consider the tetrad $e^\mu{}_{(\alpha)}$ associated to a static observer in the space-time (1), such that the line element takes the form

$$ds^2 = \eta_{\alpha\beta}d\xi^{(\alpha)}d\xi^{(\beta)} \ , \tag{18}$$

where $\eta_{\alpha\beta} = {\rm diag}(-1,1,1,1)$ is the flat-space metric tensor, and $d\xi^{(\alpha)} = e^{(\alpha)}{}_\mu dx^\mu$. We immediately note from Eq. (1) that for $e^{(1)}{}_\mu$ and $e^{(2)}{}_\mu$ the basis vectors reduce to:

$$e^{(1)}{}_\mu = \left(0, \frac{r}{\Delta^{1/2}}\left[1 + \frac{r^2 fh}{2\Delta}\right], 0, 0\right) \ , \tag{19}$$

$$e^{(2)}{}_\mu = (0,0,r,0) \ . \tag{20}$$

[1] Hereafter indices within round brackets will refer to tetrad components.

The other two components can be derived from the orthogonality condition $\eta_{\alpha\beta}e^{(\alpha)}{}_{\mu}e^{(\alpha)}{}_{\mu} = g_{\mu\nu}$, from which we find:

$$e^{(0)}{}_{\mu} = \left(f[1+h/2], 0, 0, \frac{2aM}{rf}[1+h/2]\right) \ , \tag{21}$$

$$e^{(3)}{}_{\mu} = \left(0, 0, 0, \frac{\sqrt{\Delta}}{f} + \frac{a^2 h}{2f\Delta^{1/2}}\right) \ , \tag{22}$$

where $f = \sqrt{1-2M/r}$.

The parallel transported tetrad can be now obtained applying to $\lambda^{\mu}{}_{(\alpha)}$ a Lorentz boost along the 3-direction, such that the time component of the new reference frame coincides with the test particle 4-velocity u^{μ}. The new basis vectors on the worldline read

$$\lambda^{\mu}{}_{(0)} = \gamma\left[e^{\mu}{}_{(0)} + \beta e^{\mu}{}_{(3)}\right] \quad , \quad \lambda^{\mu}{}_{(1)} = e^{\mu}{}_{(1)} \ , \tag{23}$$

$$\lambda^{\mu}{}_{(2)} = e^{\mu}{}_{(2)} \quad , \quad \lambda^{\mu}{}_{(3)} = \gamma\left[e^{\mu}{}_{(0)} + \beta e^{\mu}{}_{(3)}\right] \ , \tag{24}$$

where β and γ are the boost velocity and the corresponding Lorentz factor. They can be easily obtained from the condition $\lambda^{\mu}{}_{(0)} = u^{\mu}$, from which we find:

$$\begin{aligned}\gamma =& \frac{1}{Nf}[1+\omega_{\rm k}(a-2r^2\omega_{\rm k})] - \frac{h}{4r^2N^3f}\left[6a^3\omega_{\rm k}\right. \\ &+ a^2(3-8r^2\omega_{\rm k}^2) + 2ar^2\omega_{\rm k}(3-5r^2\omega_{\rm k}^2) \\ &\left.+3r^2(1-2r^2\omega_{\rm k}^2)^2\right] \ ,\end{aligned} \tag{25}$$

$$\begin{aligned}\beta =& \frac{\omega_{\rm k}\Delta^{1/2}}{1+\omega_{\rm k}(a-2r^2\omega_{\rm k})} - \frac{hf^2}{4\omega_{\rm k}}\frac{\Delta^{-1/2}}{(r+ar\omega_{\rm k}-2M)^2} \\ &\times\left[a^2(3-8r^2\omega_{\rm k}^2) + 2ar^2\omega_{\rm k}(3-5r^2\omega_{\rm k}^2)\right. \\ &\left.+6a^3\omega_{\rm k} + 3r^2f^4\right] \ .\end{aligned} \tag{26}$$

The time component of the tetrad $\lambda^{\mu}{}_{(0)}$ is automatically parallel transported along the particle wordline, as the vector $\lambda^{\mu}{}_{(2)}$. However the two spatial vectors $\lambda^{\mu}{}_{(1)}$ and $\lambda^{\mu}{}_{(3)}$, which in spherical polar coordinates are along the radial and tangential direction with respect to the orbit, must to be rotated to be parallel propagated. Therefore, we introduce two new vectors $\tilde{\lambda}^{\mu}{}_{(1)}, \tilde{\lambda}^{\mu}{}_{(3)}$ defined as:

$$\tilde{\lambda}^{\mu}{}_{(1)} = \lambda^{\mu}{}_{(1)}\cos\xi - \lambda^{\mu}{}_{(3)}\sin\xi \ , \tag{27}$$

$$\tilde{\lambda}^{\mu}{}_{(3)} = \lambda^{\mu}{}_{(1)}\sin\xi + \lambda^{\mu}{}_{(3)}\cos\xi \ . \tag{28}$$

Requiring that $\tilde{\lambda}^{\mu}{}_{(1)}$ and $\tilde{\lambda}^{\mu}{}_{(3)}$ and satisfy the parallel transport equation along the wordline with tangent vector $\lambda^{\mu}{}_{(0)}$

$$\lambda^{\nu}{}_{(0)}(\nabla_{\nu}\tilde{\lambda}^{\mu}{}_{(1)}) = \lambda^{\nu}{}_{(0)}(\nabla_{\nu}\tilde{\lambda}^{\mu}{}_{(3)}) = 0 \ , \tag{29}$$

yields for the ξ:

$$\xi = \omega_{\rm k}\tau\left(1 - \frac{3r-4M}{4M}h\right) \ , \tag{30}$$

having fixed the integration constant such that $\xi(\tau = 0) = 0$. The full expression for the basis vectors $(\lambda^{\mu}{}_{(0)}, \tilde{\lambda}^{\mu}{}_{(1)}, \lambda^{\mu}{}_{(2)}, \tilde{\lambda}^{\mu}{}_{(3)})$ at the linear order in h is given in Appendix A.

Having computed the parallel transported tetrad we can now project the $R_{\alpha\beta\gamma\delta}$ to derive the gravito-electric and gravito-magnetic tensors (15)-(16). For sake of clarity we split the each component as sum of two pieces: one related to the pure Kerr geometry, and one corresponding to the corrections induced by the parameter h in the JP metric:

$$\mathcal{E}_{(i)(j)} = \bar{\mathcal{E}}_{(i)(j)} + h\ \delta\mathcal{E}_{(i)(j)} \ , \tag{31}$$

where

$$\bar{\mathcal{E}}_{(1)(1)} = \omega_{\rm k}^2\left(1 - \frac{3}{r^2}\frac{\Delta}{N^2}\cos^2\xi\right) \ , \tag{32}$$

$$\bar{\mathcal{E}}_{(2)(2)} = \frac{\omega_{\rm k}^2}{N^2}\left(1 + 3\frac{a^2}{r^2} - 4a\omega_{\rm k}\right) \ , \tag{33}$$

$$\bar{\mathcal{E}}_{(3)(3)} = \omega_{\rm k}^2\left(1 - \frac{3}{r^2}\frac{\Delta}{N^2}\sin^2\xi\right) \ , \tag{34}$$

$$\bar{\mathcal{E}}_{(1)(3)} = -\frac{3}{2}\frac{\Delta}{N^2r^2}\omega_{\rm k}^2\sin 2\xi \ , \tag{35}$$

being $\bar{\mathcal{E}}_{22} = -(\bar{\mathcal{E}}_{11} + \bar{\mathcal{E}}_{33})$ and ξ given by Eq. (30). The changes to the electric tidal tensor induced by the strong field deviations read:

$$\delta\mathcal{E}_{(1)(1)} = \frac{4\omega_{\rm k}^2 r^2 - 3}{2r^2}\sin^2\xi + \frac{1}{2r^4N^4}\left[3(5a^2+4r^2) + (51a^3+39ar^2)\omega_{\rm k} + (42a^4 - 48a^2r^2 - 80r^4)\omega_{\rm k}^2 \right.$$
$$\left. -2(66a^3r^2 + 85ar^4)\omega_{\rm k}^3 + (40a^2r^4 + 183r^6)\omega_{\rm k}^4 + 192ar^6\omega_{\rm K}^5 - 144r^8\omega_{\rm k}^6\right]\cos^2\xi \ , \quad (36)$$

$$\delta\mathcal{E}_{(2)(2)} = \frac{1}{N^4r^2}\left[-\frac{3}{2}\left(3+\frac{5a^2}{r^2}\right) - \frac{3}{2}a\left(9+\frac{17a^2}{r^2}\right)\omega_{\rm k} + \left(30a^2 - \frac{21a^4}{r^2} + 29r^2\right)\omega_{\rm K}^2 + (66a^3+59ar^2)\omega_{\rm k}^3 \right.$$
$$\left. -(28a^2r^2+66r^4)\omega_{\rm k}^4 - 72ar^4\omega_{\rm k}^5 + 54\omega_{\rm k}^6r^6\right] \ , \quad (37)$$

$$\delta\mathcal{E}_{(3)(3)} = \frac{4\omega_{\rm k}^2 r^2 - 3}{2r^2}\cos^2\xi + \frac{1}{2r^4N^4}\left[3(5a^2+4r^2) + (51a^3+39ar^2)\omega_{\rm k} + (42a^4 - 48a^2r^2 - 80r^4)\omega_{\rm k}^2 \right.$$
$$\left. -2(66a^3r^2 + 85ar^4)\omega_{\rm k}^3 + (40a^2r^4 + 183r^6)\omega_{\rm k}^4 + 192ar^6\omega_{\rm K}^5 - 144r^8\omega_{\rm k}^6\right]\sin^2\xi \ , \quad (38)$$

$$\delta\mathcal{E}_{(1)(3)} = \frac{1}{N^4r^4}\left[\frac{15}{4}(a^2+r^2) + \frac{51}{4}a(r^2+a^2)\omega_{\rm k} + \frac{3}{2}(7a^4 - 6a^2r^2 - 17r^4)\omega_{\rm k}^2 - \frac{3}{2}(22a^3r^2+37ar^4)\omega_{\rm k}^3 \right.$$
$$\left. +\left(6a^2r^4 + \frac{117}{2}r^6\right)\omega_{\rm k}^4 + 60ar^6\omega_{\rm k}^5 - 45r^8\omega_{\rm k}^6\right]\sin 2\xi \ . \quad (39)$$

Similarly, the non vanishing components of the magnetic term (16) are :

$$\bar{\mathcal{H}}_{(1)(2)} = -3\frac{\omega_{\rm k}^2}{r^2}(\omega_{\rm k}r^2 - a)\frac{\Delta^{1/2}}{N^2}\cos\xi \ , \quad (40)$$

$$\bar{\mathcal{H}}_{(2)(3)} = -3\frac{\omega_{\rm k}^2}{r^2}(\omega_{\rm k}r^2 - a)\frac{\Delta^{1/2}}{N^2}\sin\xi \ , \quad (41)$$

and finally,

$$\delta\mathcal{H}_{(1)(2)} = -\frac{\Delta^{-1/2}}{r^2N^4}\left[\left(33a^2 + \frac{18a^4}{r^2} + 11r^2\right)\frac{\omega_{\rm k}}{4} + \left(\frac{27}{2}a^3 + \frac{9a^5}{r^2} + 2ar^2\right)\omega_{\rm k}^2 - \frac{\omega_{\rm k}^3}{4}\left(72a^4 + 163a^2r^2 + 55r^4\right)\right.$$
$$\left. -\left(18a^3r^2 - \frac{ar^4}{2}\right)\omega_{\rm k}^4 + (47a^2r^4 + 21r^6)\omega_{\rm k}^5 - 9ar^6\omega_{\rm k}^6 - 9r^8\omega_{\rm k}^7\right]\cos\xi \ , \quad (42)$$

$$\delta\mathcal{H}_{(2)(3)} = -\frac{\Delta^{-1/2}}{r^2N^4}\left[\left(45a^2 + \frac{18a^4}{r^2} + 27r^2\right)\frac{\omega_{\rm k}}{4} + \left(\frac{51a^3}{2} + \frac{9a^5}{r^2} + 15ar^2\right)\omega_{\rm k}^2 - \left(24a^4 + 195a^2r^2 + 171r^4\right)\frac{\omega_{\rm k}^3}{4}\right.$$
$$\left. -\left(54a^3r^2 + \frac{117ar^4}{2}\right)\omega_{\rm k}^4 + (54a^2r^4 + 90r^6)\omega_{\rm k}^5 + 57ar^6\omega_{\rm k}^6 - 63r^8\omega_{\rm k}^7\right]\sin\xi \ . \quad (43)$$

A. Relevance of strong-gravity corrections

Given the explicit form of the gravito-magnetic and electric tidal tensors Eqns. (32)-(43), we need to estimate the relevance of the non-Kerr components as function of the BH angular momentum and the deformation parameter ϵ_3. To this aim we define the two quantities

$$\Delta\mathcal{E}_{ij} = h\frac{\delta\mathcal{E}_{(i)(j)}}{\bar{\mathcal{E}}_{(i)(j)}} \qquad \text{and} \qquad \Delta\mathcal{H}_{ij} = h\frac{\delta\mathcal{H}_{(i)(j)}}{\bar{\mathcal{H}}_{(i)(j)}} \ , \quad (44)$$

which represent the fractional change with respect to $\mathcal{E}$ and $\mathcal{H}$ computed in the standard GR scenario. In the following, starting from an initial configuration with $\xi(\tau_0) = 0$, we consider snapshots at different orbital distances with the same phase $\xi(\tau) = \xi(\tau_0)$. Even though a more accurate analysis well be developed in the next section through a numerical approach, this assumption will provide, as first hint, an order of magnitude estimate of the effects we are going to study. We note that in this case $\mathcal{E}_{(1)(3)} = \mathcal{H}_{(2)(3)} = 0$. Our results can be summarised in Figures 2-4.

In the three panels of Fig. 2 we show the absolute value of $\Delta\mathcal{E}_{ij}$ as function of the orbital distance, for $\epsilon_3 = (1, 5, 10)$ and BH spin parameter $a/M = 0.5$. As expected, the contribution of strong gravity terms grow as

r decreases and can be of the order $\sim 10\%$ for $r > 10M$. For $r < 6M$ and $\epsilon_3 > 5$ the relative difference is always larger than 50%: terms of second order $\mathcal{O}(h^2)$ and proportional to higher coefficients as ϵ_4 start to be relevant, and cannot be neglected. For $\epsilon_3 > 0$ (< 0 respectively) all the components of $\Delta\mathcal{E}_{ij}$ are smaller (higher) than zero, and therefore the strong-gravity corrections reduce (increase) the neat effect of tidal deviations induced by the gravito-electric tensor[2].

In Fig. 3 we draw $\Delta\mathcal{E}_{11}$ for $\epsilon_3 = 10$ and different values of $a/M = (0.1, 0.5, 0.8)$. The plot shows that unless the binary systems gets very close at orbital distances $r \ll 10M$, the effects of non-Kerr deviations seem to be insensitive to the BH spin. This feature does not change for the other components of $\mathcal{E}_{(i)(j)}$.

Finally, we note that the picture described above also apply to the gravito-magnetic tidal tensor. We show the behaviour of $\Delta\mathcal{H}_{12}$ in Fig. 4-5 for the same set of parameters previously considered.

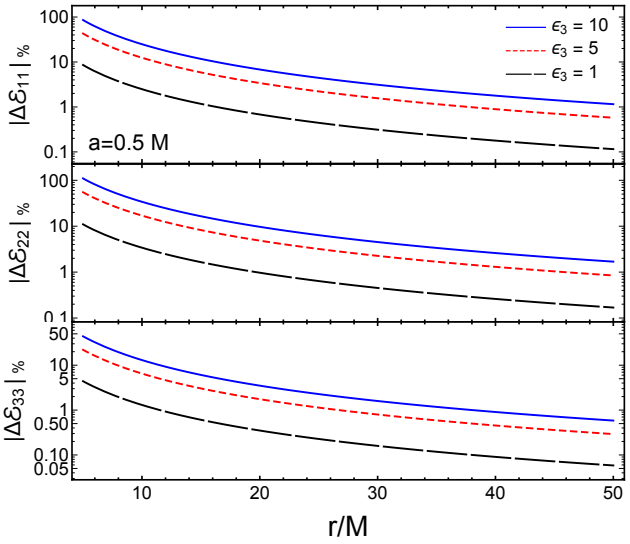

Figure 2. In this figure we plot the absolute percentage values of $\Delta\mathcal{E}_{ij}$ given by Eq. (44) as function of the orbital distance, for three values of the strong gravity parameter $\epsilon_3 = (1, 5, 10)$, and BH spin $a = 0.5M$.

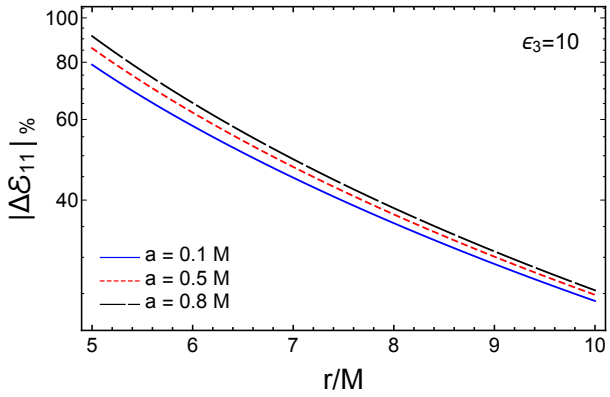

Figure 3. Same as Fig. 2 but only for $\Delta\mathcal{E}_{11}$, with $\epsilon_3 = 10$ and different values of the BH spin parameter $a/M = (0.1, 0.5, 0.8)$.

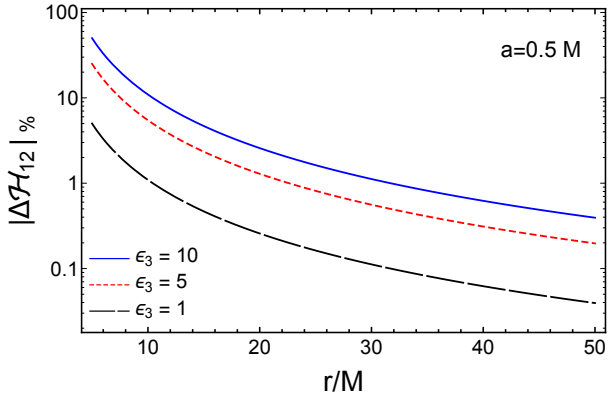

Figure 4. Same as Fig. 2 but for the magnetic component $\Delta\mathcal{H}_{12}$.

IV. BLACK HOLE - WHITE DWARF BINARY EVOLUTION

Hereafter we will analyse the effects of strong-field corrections derived in the previous section, using our results together with the affine model, which represents a semi-analytic approach to describe stellar deformations induced by an external tidal field. We shall first provide a brief summary of the main ingredients of the model, referring the reader to [34] (reference therein) for a more comprehensive description of this framework. Then, we will present the numerical results obtained for different configurations of prototype BH-white dwarf (WD) binaries.

A. The model

The main assumption of the affine approach is that the spherical star is deformed by the tidal field into an ellipsoid, preserving this shape during the orbital motion. More specifically, it is warped in an S-type Riemann ellipsoid, for which the spin and vorticity are parallel, and their ratio constant [45]. The equations for the stellar deformations are written in the *principal frame*, which is comoving with the star, and such that the axes are

[2] This feature could be qualitatively expected since for $\epsilon_3 > 0$ ($\epsilon_3 < 0$) the modified BH is more prolate (oblate) than the Kerr one [20].

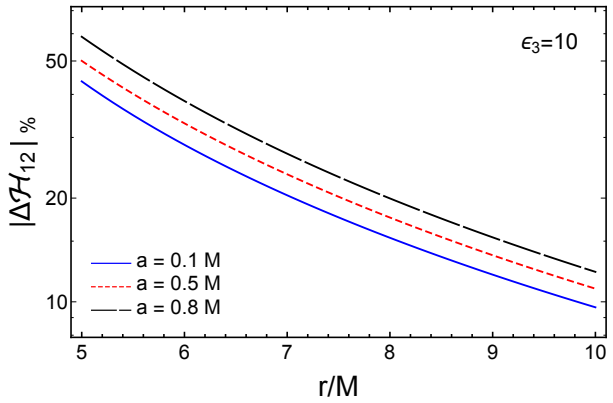

Figure 5. Same as Fig. 3 but for the magnetic component $\Delta\mathcal{H}_{12}$.

adapted to the principal axes of the ellipsoid [3] $a_{i=1,2,3}$. Under this assumption, the infinite number of degrees of freedom of the internal fluid, is reduced to a set of five variables $(a_1, a_2, a_3, \psi, \lambda)$, where ψ and λ are the two angles:

$$\frac{d\psi}{d\tau} = \Omega \qquad , \qquad \frac{d\lambda}{d\tau} = \Lambda \ . \tag{45}$$

In the previous expressions, Ω is the WD angular velocity measured in the tetrad coordinate system (which is parallel transported), and Λ describes the internal fluid motion in the principal frame.

The equations of motion for the star can be derived from the Lagrangian

$$\mathcal{L} = \mathcal{L}_{\rm B} + \mathcal{L}_{\rm T} \ , \tag{46}$$

where the subscripts T and B refer to *tidal* and *body*. The first term reads:

$$\mathcal{L}_{\rm T} = -\frac{1}{2} c_{ij} I_{ij} \ , \tag{47}$$

where I_{ij} s the inertial tensor, which is written in the affine model as :

$$I_{ij} = \hat{\mathcal{M}} \cdot {\rm diag}\left(\frac{a_i}{R_{\rm WD}}\right)^2 = \frac{4\pi}{3}\int_0^{R_{\rm WD}} \hat{\rho}(r) r^4 dr \ , \tag{48}$$

being $\hat{\mathcal{M}}$ the scalar quadrupole moment computed over the density profile of the star[4], and $R_{\rm WD}$ its radius at spherical equilibrium. c_{ij} are the components of the gravito-electric tidal tensor in the principal frame, obtained by rotating $\mathcal{E}_{ij}$ of the angle ψ (defined in Eq. (45)) $c = T\mathcal{E}T^T$, where the matrix T is given by:

$$T = \begin{pmatrix} \cos\psi & 0 & \sin\psi \\ 0 & 1 & 0 \\ -\sin\psi & 0 & \cos\psi \end{pmatrix} \ . \tag{49}$$

Practically speaking, this rotation changes the angle ξ into $l = \psi - \xi$. The latter describes the misalignment between the a_1 axis and the line between the two objects: when l is negligible, the binary is said to be *synchronised*. For a star with zero viscosity this angle is in general very small. However, as the orbit shrinks the tidal bulge lags behind the tidal potential, and then is subject to a torque which tries to spin it to follow the orbital motion, and the system de-synchronises [46, 47].

The body Lagrangian $\mathcal{L}_{\rm B}$ describes the star internal dynamics, and contains three contributions coming from the kinetic, the internal energy of the fluid, and the self gravity (see [34] for a complete expression of these quantities in terms of the affine model variables). By applying the Euler-Lagrange formalism to Eq. (46) we obtain the equations of motion for the star:

$$\begin{aligned} \ddot{a}_1 =& a_1(\Lambda^2 + \Omega^2) - 2a_2\Lambda\Omega + \frac{1}{2}\frac{\hat{V}}{\hat{\mathcal{M}}} R_{\rm WD}^3 a_1 A_1 \\ & - \frac{R_{\rm WD}^2}{\mathcal{M}}\frac{\hat{V}}{3a_1} - c_{11}a_1 \ , \end{aligned} \tag{50}$$

$$\begin{aligned} \ddot{a}_3 =& a_3(\Lambda^2 + \Omega^2) - 2a_1\Lambda\Omega + \frac{1}{2}\frac{\hat{V}}{\hat{\mathcal{M}}} R_{\rm WD}^3 a_3 A_3 \\ & - \frac{R_{\rm WD}^2}{\hat{\mathcal{M}}}\frac{\hat{V}}{3a_3} - c_{33}a_3 \ , \end{aligned} \tag{51}$$

$$\ddot{a}_2 = \frac{1}{2}\frac{\hat{V}}{\hat{\mathcal{M}}} R_{\rm WD}^3 a_2 A_2 - \frac{R_{\rm WD}^2}{\hat{\mathcal{M}}}\frac{\hat{V}}{3a_2} - c_{22}a_2 \ , \tag{52}$$

$$\dot{J} = \frac{\hat{\mathcal{M}}}{R_{\rm WD}^2} c_{13}(a_3^2 - a_1^2) \ , \tag{53}$$

$$\dot{\mathcal{C}} = 0 \ , \tag{54}$$

where dot refers to differentiation with respect to the proper time τ, and $\hat{V}$ is the star self-gravity at spherical equilibrium, given by

$$\hat{V} = -\frac{G}{2}\int_{\rm spher} r\partial_r \Phi_{\rm Newt} dm \ , \tag{55}$$

with $\Phi_{\rm Newt}$ Newtonian gravitational potential and dm WD mass element. We have also introduced the quantities

$$A_i = \int_0^\infty \frac{du}{(a_i^2 + u)\sqrt{(a_1^2+u)(a_2^2+u)(a_3^2+u)}} \ , \tag{56}$$

$$J = \frac{\hat{\mathcal{M}}}{R_{\rm WD}^2}[(a_1^2 + a_3^2)\Omega - 2a_1a_3\Lambda] \ , \tag{57}$$

$$\mathcal{C} = \frac{\hat{\mathcal{M}}}{R_{\rm WD}^2}[(a_1^2 + a_3^2)\Lambda - 2a_1a_3\Omega] \ , \tag{58}$$

[3] In the following "1" denotes the direction along the axis parallel to the orbital separation, "2" identifies the axis orthogonal to the orbital plane, and "3" defines the other axis in the orbital plane.

[4] The superscript hat denotes quantities computed for the spherical star.

being J the star angular momentum, and $\mathcal{C}$ the circulation of the fluid [30]. In absence of viscosity, as for the models we are going to study here, $\mathcal{C}$ is a constant of motion. We also consider irrotational configurations, for which $\mathcal{C} = 0$.

In this work we investigate quasi-equilibrium sequences of BH-WD binaries: this assumption reduces Eqns (50)-(54) to a system of coupled algebraic equations:

$$\ddot{a}_i = 0 \quad , \quad \psi = \xi \quad , \quad \dot{\psi} = \Omega = \dot{\xi} \, , \tag{59}$$

which is solved through a Newton-Raphson method.

B. Numerical results

We employ the affine model for a representative set of binary configurations. The WD equilibrium structure is build within a Newtonian framework using a polytropic equation of state $P = K\rho^{\gamma}$ with $\gamma = 4/3$, where P and ρ are the pressure and mass-density profiles. We choose the central density and the constant K such that the star has mass and radius $M_{\rm WD} = 1 M_{\odot}$ and $R_{\rm WD} = 7088$ km. Moreover, we consider rotating BHs with mass $M = 10^4 M_{\odot}$, spins $a = (0.5, 0.8)M$, and five values for the deformation parameter of the JP metric $\epsilon_3 = (0, \pm 5, \pm 10)$. For each configuration, we solve the system of Eqns. (59) placing the spherical star at the orbital separation $r \gg R_{\rm WD}$ from the BH. Then, we gradually reduce the distance until it reaches the critical point $r_{\rm tide}$ at which the WD fills its Roche Lobe. The latter defines the region around the star in which a particle with mass $m \ll M_{\rm WD}$ is gravitationally bounded to the central object. At the Newtonian level, the Roche lobe can be identified finding the maximum of the three-body potential (in the equatorial plane x-y):

$$U(x,y) = -\frac{G m_1}{|\vec{x} - \vec{y}_1|} - \frac{G m_1}{|\vec{x} - \vec{y}_2|} - \frac{G}{2}\frac{(m_1 + m_2)}{|\vec{y}_1 - \vec{y}_2|^3} x^2 \, , \tag{60}$$

where $\vec{y}_{1/2}$ are the displacement vectors, and in our case $m_1 = M$, $m_2 = M_{\rm WD}$. At each step of the simulation we numerically compute Eq. (60) and its maximum, defining $r_{\rm tide}$ as the orbital distance for which the WD axis a_1, elongated by the tidal forces, touches the Roche lobe.

Our results can be summarised as follows:

- In Fig. 6 we show the relative difference between the axes a_1, a_2 computed for $\epsilon_3 = (\pm 5, \pm 10)$ and $\epsilon_3 = 0$, namely:

$$\Delta a_1 = \frac{a_1\big|_{\epsilon_3 = \pm 5}}{a_1\big|_{\epsilon_3 = 0}} - 1 \quad , \quad \Delta a_1 = \frac{a_1\big|_{\epsilon_3 = \pm 10}}{a_1\big|_{\epsilon_3 = 0}} - 1 \, , \tag{61}$$

  as function of the orbital distance normalised to the BH mass, for $a/M = 0.5$. This quantity is evaluated up to the radius[5] $r_{\rm tide}\big|_{\epsilon_3 = 0}$ or $r_{\rm tide}\big|_{\epsilon_3 = -5, -10}$, for positive and negative values of ϵ_3, respectively. As the relative separation shrinks, the difference between the GR and the alternative scenario increases up to $\sim 3\%$ and $\sim 5\%$ for $\epsilon_3 = \pm 5$ and $\epsilon_3 = \pm 10$, respectively. The effect on the axis a_2 is less pronounced with discrepancies smaller than 1%; the same results apply to the axis a_3.

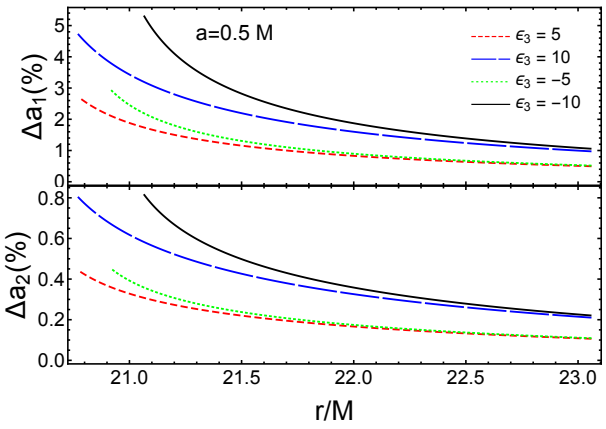

Figure 6. We show the difference Eq. (61), between the axes computed for $\epsilon_3 = (\pm 5, \pm 10)$ and $\epsilon_3 = 0$, for $a/M = 0.5$, as function of the orbital distance divided by the total mass of the system.

- In Table I we show, for each binary configuration considered, the critical distances at which the WD fills its Roche lobe, and the related values of the axes normalised to the star radius at spherical equilibrium, $\bar{a}_i = a_i / R_{\rm WD}$. We note that all the simulations end around $r_{\rm tide} \sim 20 M_{\rm tot}$. This can be explained looking at the behaviour of the gravito-electric tidal tensor in Fig. 1, which shows that the effect of the deformation parameter ϵ_3 plays a crucial role only for distances $r \sim 10 M_{\rm tot}$. Finally, as pointed out in the previous section, values of ϵ_3 smaller than zero increase the strength of the tidal field, and make the star filling its Roche Lobe at larger distances.

  It is worth remarking that the orbital radius $r_{\rm tide}$ does not identify the WD tidal disruption, but the distance at which the star begins to loose mass towards the companion object. We expect therefore, that the orbital evolution after this critical point, and the dynamics of the accreting flow, will be significantly affected by the Kerr metric modifications. However, such effects can be tracked only by means of numerical codes. This will be the subject of further investigations, in which we will implement the

[5] As noted in Sec. III A, values of the parameter ϵ_3 greater than zero reduce the effect of the tidal field, and then make the star filling its Roche lobe at smaller orbital distances than the pure GR case for which $\epsilon_3 = 0$. Viceversa, for $\epsilon_3 < 0$ the star touches the Roche Lobe surface earlier.

theoretical results developed in the previous section into fully relativistic numerical simulations.

a	ϵ_3	$r_{\rm tide}/M$	$\bar{a}_1$	$\bar{a}_2$	$\bar{a}_3$
0.5	0	20.773	1.306	0.919	0.947
0.5	5	20.621	1.296	0.919	0.948
0.5	10	20.464	1.287	0.920	0.949
0.5	-5	20.922	1.315	0.919	0.946
0.5	-10	21.066	1.323	0.919	0.945
0.8	0	20.738	1.303	0.919	0.947
0.8	5	20.584	1.294	0.919	0.949
0.8	10	20.426	1.285	0.919	0.950
0.8	-5	20.888	1.312	0.919	0.946
0.8	-10	21.033	1.321	0.918	0.945

Table I. For each binary configuration considered, identified by the BH spin a/M and the deformation parameter ϵ_3, we show the critical orbital distance at which the simulation ends, and the maximum deformation of the WD axes normalised to its radius at spherical equilibrium $\bar{a}_i = a_i/R_{\rm WD}$.

- We have followed the same procedure described above for $a/M = 0.8$, finding again differences at the most of $\Delta a_1 \sim 5\%$ for $\epsilon_3 = \pm 10$. As already noted therefore, the effect of the BH spin does not change the evolutionary picture. This can be easily understood looking at Eqns. (32)-(35): even in the standard Kerr case, the spin starts to provide a significant contribution only for distances $r < 10M$.

V. CONCLUSIONS

Current and future observations in the electromagnetic and gravitational spectrum will allow to map the spacetime around supermassive BHs, and to study the properties of the strong gravitational field in their surroundings. In particular, these experiments will shed new light on the validity of the no-hair theorem, for which astrophysical BHs in General Relativity belong to the Kerr family, and are described only by their mass and spin. In this scenario, the quest for model independent tests of gravity which make use of the incoming flood of data, is more needed than ever. Several efforts have been devoted to pursue this goal. Among the model proposed in literature, we have considered the JP metric, which parametrises the deviations from the Kerr geometry through a set of free parameters, to be constrained by experiments.

In this work we focused our attention on the description of tidal effects produced by rotating BHs. We computed the analytic expression for the gravito-magnetic and gravito-electric tidal tensors, which completely describe the quadrupolar nature of the tidal field. We consider the case of equatorial geodesics, expanding all quantities at the linear order in the parameter ϵ_3 (or equivalently h), which identifies the deviations from the Kerr metric. Comparing our results with those obtained in the pure GR case, we have found discrepancies both for $\mathcal{E}$ and $\mathcal{H}$ which can be as high as $\sim 10\%$ even for large distances, $r > 10M$. These differences seems also to weakly depend on the BH angular momentum.

We have implemented our results into a semi-analytic approach, called the affine model, to simulate the encounter of BH-WD systems, following the orbital evolution until the star fill its Roche lobe. Analysing a representative set of binary configurations, we have found that the tidal deformations of the WD can be up to 5% different between the pure GR and the alternative scenario, for $\epsilon_3 = \pm 10$, even at orbital separation $r \sim 20M$. Therefore, we expect that the matter flow onto the BH, and the possible formation of an accreting disk, would be significantly affected by the strong field correction induced by the JP metric.

Assessing the features and the detectability of such processes will be matter of future investigations, in which we will implement our theoretical results into fully relativistic numerical simulations.

ACKNOWLEDGMENTS

It is a pleasure to thank Cosimo Bambi for having carefully read the manuscript and for his useful comments. P.L. is supported by the NSF grants 1505824 and 1333360.

Appendix A: The parallel transported tetrad in the JP space-time

In this section we show the form of the basis vectors $\lambda^\mu{}_{(\alpha)}$ parallel propagated along a circular geodesic in the JP space-time, at the linear order in the parameter $h = \epsilon_3 M^3/r^3$.

$$\lambda^0{}_{(0)} = \frac{1 + a\omega_{\rm k}}{N} - \frac{h}{N^3 4r^2}\left[3a^2 + 5r^2 + 6a(a^2+r^2)\omega_{\rm k} - 4r^2(4a^2+3r^2)\omega_{\rm K}^2 + 12ar^4\omega_{\rm k}^3\right] , \tag{A1a}$$

$$\lambda^1{}_{(0)} = 0 , \tag{A1b}$$

$$\lambda^2{}_{(0)} = 0 , \tag{A1c}$$

$$\lambda^3{}_{(0)} = \frac{\omega_{\rm k}}{N} - \frac{h}{4r^2\omega_{\rm k}N^3}\left[6a^2\omega_{\rm k}^2 + a\omega_{\rm k}(9 - 16r^2\omega_{\rm k}^2) + 3(1 - 2r^2\omega_{\rm k}^2)^2\right] , \tag{A1d}$$

$$\tilde{\lambda}^{0}{}_{(1)} = -\frac{\sqrt{\Delta}\omega_{\rm k}}{N}\sin\xi + \frac{h\Delta^{-3/2}}{4r^2N^3\omega_{\rm k}}\left[(a^2+r^2)^2(3+9a\omega_{\rm k}) + 2(a^2+r^2)\omega_{\rm k}^2(3a^4-8r^4) - 4ar^2\omega_{\rm k}^3(a^4+11a^2r^2 + 9r^4) + 2r^4(13r^4-3a^2r^2-18a^4)\omega_{\rm k}^4 + 8ar^6(5a^2+6r^2)\omega_{\rm k}^5 + 4r^8(5a^2-3r^2)\omega_{\rm k}^6 - 24ar^{10}\omega_{\rm k}^7\right]\sin\xi \ , \tag{A2a}$$

$$\tilde{\lambda}^{1}{}_{(1)} = \frac{\Delta^{1/2}}{r}\cos\xi - \frac{h}{2\Delta^{1/2}}(r-2M)\cos\xi \ , \tag{A2b}$$

$$\tilde{\lambda}^{2}{}_{(1)} = 0 \ , \tag{A2c}$$

$$\tilde{\lambda}^{3}{}_{(1)} = -\frac{1+\omega_{\rm k}(a-2r^2\omega_{\rm k})}{N\Delta^{1/2}}\sin\xi + \frac{h}{4r^2N^3\Delta^{3/2}}\left[6a^5\omega_{\rm k} + a^4(3-4r^2\omega_{\rm k}^2) + 18a^3r\omega_{\rm k}(r-2M) + 3r(r-2M)^3 + 4a^2r^2(2-9r^2\omega_{\rm k}^2+10r^4\omega_{\rm k}^4) + a(6r^4\omega_{\rm k} - 22r^6\omega_{\rm k}^3 + 20r^8\omega_{\rm k}^5)\right]\sin\xi \ , \tag{A2d}$$

$$\lambda^{0}{}_{(2)} = 0 \ , \tag{A3a}$$

$$\lambda^{1}{}_{(2)} = 0 \ , \tag{A3b}$$

$$\lambda^{3}{}_{(2)} = 0 \ , \tag{A3c}$$

$$\lambda^{2}{}_{(2)} = \frac{1}{r} \ , \tag{A3d}$$

$$\tilde{\lambda}^{0}{}_{(3)} = \frac{\sqrt{\Delta}\omega_{\rm k}}{N}\cos\xi - \frac{h\Delta^{-3/2}}{4r^2N^3\omega_{\rm k}}\left[(a^2+r^2)^2(3+9a\omega_{\rm k}) + 2(a^2+r^2)\omega_{\rm k}^2(3a^4-8r^4) - 4ar^2\omega_{\rm k}^3(a^4+11a^2r^2 + 9r^4) + 2r^4(13r^4-3a^2r^2-18a^4)\omega_{\rm k}^4 + 8ar^6(5a^2+6r^2)\omega_{\rm k}^5 + 4r^8(5a^2-3r^2)\omega_{\rm k}^6 - 24ar^{10}\omega_{\rm k}^7\right]\cos\xi \ , \tag{A4a}$$

$$\tilde{\lambda}^{1}{}_{(3)} = -\frac{\Delta^{1/2}}{r}\sin\xi - \frac{h}{2\Delta^{1/2}}(r-2M)\sin\xi \ , \tag{A4b}$$

$$\tilde{\lambda}^{2}{}_{(3)} = 0 \ , \tag{A4c}$$

$$\tilde{\lambda}^{3}{}_{(3)} = \frac{1+\omega_{\rm k}(a-2r^2\omega_{\rm k})}{N\Delta^{1/2}}\cos\xi - \frac{h}{4r^2N^3\Delta^{3/2}}\left[6a^5\omega_{\rm k} + a^4(3-4r^2\omega_{\rm k}^2) + 18a^3r\omega_{\rm k}(r-2M) + 3r(r-2M)^3 + 4a^2r^2(2-9r^2\omega_{\rm k}^2+10r^4\omega_{\rm k}^4) + a(6r^4\omega_{\rm k} - 22r^6\omega_{\rm k}^3 + 20r^8\omega_{\rm k}^5)\right]\cos\xi \ . \tag{A4d}$$

[1] C. M. Will, Living Rev.Rel. **17**, 4 (2014), 1403.7377.
[2] E. Berti et al., Class. Quant. Grav. **32**, 243001 (2015), 1501.07274.
[3] N. Yunes and X. Siemens, Living Rev.Rel. **16**, 9 (2013).
[4] D. Psaltis, Living Rev.Rel. (2008), 0806.1531.
[5] C. Bambi (2015), 1509.03884.
[6] D. L. Wiltshire, M. Visser, and S. M. Scott, *The Kerr spacetime: Rotating black holes in general relativity* (Cambridge University Press, 2009).
[7] R. H. Price, Phys. Rev. D **5**, 2419 (1972), URL `http://link.aps.org/doi/10.1103/PhysRevD.5.2419`.
[8] A. E. Broderick, T. Johannsen, A. Loeb, and D. Psaltis, Astrophys. J. **784**, 7 (2014), 1311.5564.
[9] F. Eisenhauer et al., in *Society of Photo-Optical Instrumentation Engineers (SPIE) Conference Series* (2008), vol. 7013 of *Society of Photo-Optical Instrumentation Engineers (SPIE) Conference Series*, p. 2, 0808.0063.

[10] M. Feroci, L. Stella, M. Van der Klis, T.-L. Courvoisier, M. Hernanz, R. Hudec, A. Santangelo, D. Walton, A. Zdziarski, D. Barret, et al., Experimental Astronomy **34**, 415 (2012).

[11] K. C. Gendreau, Z. Arzoumanian, and T. Okajima, in *Society of Photo-Optical Instrumentation Engineers (SPIE) Conference Series* (2012), vol. 8443 of *Society of Photo-Optical Instrumentation Engineers (SPIE) Conference Series*, p. 13.

[12] G. M. Harry and the LIGO Scientific Collaboration, Class. Quantum Grav. **27**, 084006 (2010).

[13] F. Acernese et al., Class. Quantum Grav. **25**, 114045 (2008).

[14] T. Johannsen, Phys. Rev. D **87**, 124017 (2013), URL http://link.aps.org/doi/10.1103/PhysRevD.87.124017.

[15] T. Johannsen and D. Psaltis, Phys. Rev. D **83**, 124015 (2011), URL http://link.aps.org/doi/10.1103/PhysRevD.83.124015.

[16] E. T. Newman and A. I. Janis, Journal of Mathematical Physics **6** (1965).

[17] T. Johannsen and D. Psaltis, The Astrophysical Journal **716**, 187 (2010), URL http://stacks.iop.org/0004-637X/716/i=1/a=187.

[18] C. Bambi and L. Modesto, Physics Letters B **706**, 13 (2011), ISSN 0370-2693, URL http://www.sciencedirect.com/science/article/pii/S037026931101313X.

[19] C. Bambi, Phys. Rev. D **85**, 043002 (2012), URL http://link.aps.org/doi/10.1103/PhysRevD.85.043002.

[20] C. Bambi, Physics Letters B **705**, 5 (2011), ISSN 0370-2693, URL http://www.sciencedirect.com/science/article/pii/S0370269311012378.

[21] T. Johannsen, Phys. Rev. D **87**, 124010 (2013), URL http://link.aps.org/doi/10.1103/PhysRevD.87.124010.

[22] C. Bambi, Journal of Cosmology and Astroparticle Physics **2012**, 014 (2012), URL http://stacks.iop.org/1475-7516/2012/i=09/a=014.

[23] C. Bambi, Phys. Rev. D **87**, 023007 (2013), URL http://link.aps.org/doi/10.1103/PhysRevD.87.023007.

[24] T. Johannsen and D. Psaltis, Astrophys. J. **773**, 57 (2013), 1202.6069.

[25] C. Bambi, The Astrophysical Journal **761**, 174 (2012), URL http://stacks.iop.org/0004-637X/761/i=2/a=174.

[26] V. Cardoso, P. Pani, and J. a. Rico, Phys. Rev. D **89**, 064007 (2014), URL http://link.aps.org/doi/10.1103/PhysRevD.89.064007.

[27] S. Kobayashi, P. Laguna, E. S. Phinney, and P. Mészáros, The Astrophysical Journal **615**, 855 (2004), URL http://stacks.iop.org/0004-637X/615/i=2/a=855.

[28] J.-P. Luminet and J.-A. Marck, Mon. Not. Roy. Astron. Soc. **212**, 57 (1985).

[29] B. Carter and J. P. Luminet, Mon. Not. Roy. Astron. Soc. **212**, 23 (1985).

[30] P. Wiggins and D. Lai, The Astrophysical Journal **532**, 530 (2000), URL http://stacks.iop.org/0004-637X/532/i=1/a=530.

[31] V. Ferrari, L. Gualtieri, and F. Pannarale, Classical and Quantum Gravity **26**, 125004 (2009), URL http://stacks.iop.org/0264-9381/26/i=12/a=125004.

[32] V. Ferrari, L. Gualtieri, and F. Pannarale, Phys. Rev. D **81**, 064026 (2010), URL http://link.aps.org/doi/10.1103/PhysRevD.81.064026.

[33] V. Ferrari, L. Gualtieri, and A. Maselli, Phys. Rev. **D85**, 044045 (2012), 1111.6607.

[34] A. Maselli, L. Gualtieri, F. Pannarale, and V. Ferrari, Phys. Rev. **D86**, 044032 (2012), 1205.7006.

[35] C. M. Will, Living Reviews in Relativity **9** (2006), URL http://www.livingreviews.org/lrr-2006-3.

[36] C. Evans, P. Laguna, and M. Eracleous, Astrophys. J. **805**, L19 (2015), 1502.05740.

[37] G. Pappas, Mon. Not. Roy. Astron. Soc. **422**, 2581 (2012), 1201.6071.

[38] G. Pappas, Mon. Not. Roy. Astron. Soc. **454**, 4066 (2015), 1506.07225.

[39] D. Gondek-Rosi?ska, W. Klu?niak, N. Stergioulas, and M. Wi?niewicz, Phys. Rev. **D89**, 104001 (2014), 1403.1129.

[40] C. Bambi and E. Barausse, Astrophys. J. **731**, 121 (2011), 1012.2007.

[41] J. R. Gair, C. Li, and I. Mandel, Phys. Rev. **D77**, 024035 (2008), 0708.0628.

[42] C. Misner, K. Thorne, and J. Wheeler, *Gravitation* (W.H. Freeman and Company, 1973).

[43] C. Chicone and B. Mashhoon, Classical and Quantum Gravity **23**, 4021 (2006), gr-qc/0602071.

[44] F. A. E. Pirani, Acta Physica Polonica **15**, 389 (1956).

[45] S. S. Chandrasekhar, *Ellipsoidal figures of equilibrium* (New Haven : Yale University Press, 1969), ISBN 0300011164, bibliography: p. [243]-247.

[46] D. Lai, F. A. Rasio, and S. L. Shapiro, Astrophys. J. **423**, 344 (1994), astro-ph/9307032.

[47] S. Dall'Osso and E. M. Rossi, Mon. Not. Roy. Astron. Soc. **428**, 518 (2013), 1203.3440.